Quantum ghost imaging and state symmetry

Quantum ghost imaging and state symmetry

Bornman, Nicholas, Vallés, Adam, Prabhakar, Shashi, Agnew, Megan, Zhu, Feng, et al.

Nicholas Bornman, Adam Vallés, Shashi Prabhakar, Megan Agnew, Feng Zhu, Andrew Forbes, Jonathan Leach, "Quantum ghost imaging and state symmetry," Proc. SPIE 11134, Quantum Communications and Quantum Imaging XVII, 1113406 (6 September 2019); doi: 10.1117/12.2529291

SPIE.

Event: SPIE Optical Engineering + Applications, 2019, San Diego, California, United States

Quantum ghost imaging and state symmetry

Nicholas Bornman[a], Adam Vallés[a], Shashi Prabhakar[a,b], Megan Agnew[c], Feng Zhu[c], Andrew Forbes[a], and Jonathan Leach[c]

[a]School of Physics, University of the Witwatersrand, Private Bag 3, Wits 2050, South Africa
[b]CSIR National Laser Centre, P.O. Box 395, Pretoria 0001, South Africa
[c]IPaQS, SUPA, Heriot-Watt University, Edinburgh EH14 4AS, United Kingdom

ABSTRACT

Since its first demonstration in 1995, ghost imaging has provided amazing insights into both classical and quantum physics as well as having found application in, for example, microscopy and imaging under low light conditions. Traditional ghost imaging uses correlations between two photons to reconstruct an image of an object from two systems which each individually know nothing about the object. In the quantum case, the state of the two photons is typically a symmetric, entangled state. Here we investigate the effect that changing the two-photon state's symmetry has on the reconstructed object, by using Dove prisms and a Hong-Ou-Mandel filter. Interestingly, it appears that post-selecting on the anti-symmetric Bell state results in a 'double image': a juxtaposition of the original image rotated both clockwise and anti-clockwise. Furthermore, we consider a 4-photon experiment in which two photons, which originate from different entanglement sources and are hence completely independent initially, acquire correlations by way of entanglement swapping via appropriate post-selection on the remaining two photons. In such a setup, post-selecting on the symmetric Bell states results in the original object, but post-selecting on the anti-symmetric Bell state results in a contrast-reversed image of the object. These studies highlight the fundamental importance that state symmetry plays in quantum imaging.

Keywords: ghost imaging, Hong-Ou-Mandel interference, state symmetry, quantum imaging

1. INTRODUCTION

Combining potentially spacelike-separated imaging systems to form an image from an object present in only one system is the gist behind ghost imaging. After creating correlations between two photons, one photon interacts with an object and is subsequently collected by a bucket detector. No spatial information about the object can be gleaned from this photon. The other photon, which doesn't interact with the object, is collected by a spatially-resolved detector. This system also contains no object information. However, an image of the object can be reconstructed by exploiting the existence of the initial correlations created between the photons.

First demonstrated by Pittman et. al.[1] using photons entangled by way of Spontaneous Parametric Down Conversion (SPDC[2]), ghost imaging has since been observed in a variety of classical and quantum contexts. For example, classical thermal light sources[3, 4] have been employed, a computational perspective using only bucket detectors,[5] techniques using compressive sensing,[6] using different degrees of freedom (DoFs) such as time correlations[7] and the orbital angular momentum (OAM) of photons,[8] as well as two-colour ghost imaging[9] are among the many studies of this interesting phenomenon (Refs. 10, 11 give detailed reviews).

Two recent studies elucidate further interesting aspects of ghost imaging in a quantum context, namely quantum ghost imaging using entanglement-swapped photons,[12] as well as analysing the role the quantum state's symmetry has on the reconstructed image.[13] In the case of the former, two pairs of separate SPDC photons are created. By combining a photon from each pair along with appropriate post-selection and coincidence counting, the remaining photons from each pair become entangled and can subsequently be used for ghost

Send correspondence to N. B.
E-mail: nicholas.bornman1@students.wits.ac.za, Telephone: +27 11 717 6848

Quantum Communications and Quantum Imaging XVII, edited by Keith S. Deacon, Proc. of SPIE
Vol. 11134, 1113406 · © 2019 SPIE · CCC code: 0277-786X/19/$21 · doi: 10.1117/12.2529291

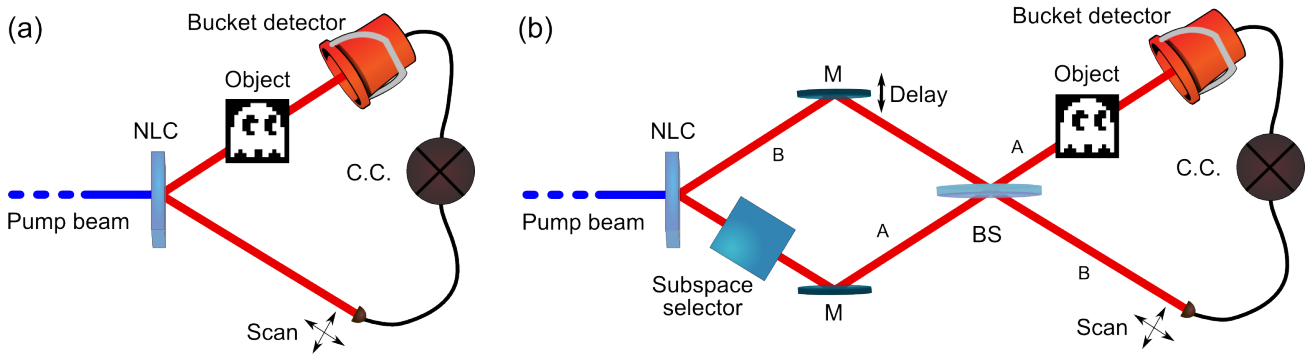

Figure 1. Schematic description of a) a traditional 2-way ghost imaging setup, and b) a modified version allowing for desired state post-selection. NLC: non-linear crystal; M: mirror; B.S.: beamsplitter; C.C.: coincidence counter.

imaging. The net result of post-selection on the anti-symmetric part of the two-photon state is the observation of a 'contrast-reversed' image of the object, i.e. pixels which were brighter in the original object appear darker in the reconstructed image, and vice-versa. This highlights the importance of better understanding state projection and state symmetry in quantum imaging. Inspired by this result, the latter study more deeply considered state symmetry and projection in a traditional two-photon ghost imaging experiment. An interesting result there was the observation that a setup using the traditional optical components of a Hong-Ou-Mandel (HOM) filter[14] results in the reconstruction of a 'double image' of the original object, in which the image is a juxtaposition of the object rotated both clockwise and anti-clockwise about its centre. Other works, such as Refs. 15, 16, have also touched on, in very different contexts, the symmetry of quantum states and its effect on entanglement and imaging.

This manuscript aims to summarise recent studies on the role that state projection and symmetry has on quantum ghost imaging, with particular reference to Refs. 12, 13.

2. 2-WAY IMAGING

2.1 Setup

Fig. 1 a) outlines a traditional ghost imaging setup. After two entangled photons are created by way of SPDC, one photon interacts with a binary object and is detected by a bucket detector. The other photon traverses a different path, being detected by a spatially-resolved detector. By counting coincidences between the two detectors, the original object can be reconstructed. This setup is modified as per Fig. 1 b) (see Ref. 13 for experimental details) by including a traditional HOM filter before the object. At the non-linear crystal plane the two entangled photons are created at the same position; in the position basis, the state is

$$|\Psi\rangle = \sum_{\boldsymbol{r}\in\mathcal{S}} c(\boldsymbol{r})\,|\boldsymbol{r}\rangle_A\,|\boldsymbol{r}\rangle_B\,, \tag{1}$$

where the sum runs over all pixels the object is comprised of (and equivalently, the corresponding spatially-resolved camera pixels in arm B, with the implicit assumption that the two are the same), a set we call $\mathcal{S}$ which has a cardinality d, and $c(\boldsymbol{r})$ is the probability amplitude for photons A and B to be found in the crystal plane at the transverse position $\boldsymbol{r} = (x, y)$ (we can set $c(\boldsymbol{r}) \equiv 1/\sqrt{d}$ for a plane wave). Note that Eq. (1) is a symmetric state.

The subspace selector (consisting of a pair of mutually-rotated Dove prisms set to an angle θ) functions as part of a quantum state engineering system and has the effect of adding a phase (depending on θ) to the photon in arm A and acts with a rotation matrix $R = R(2\theta)$ on the 2-dimensional transverse position vector, $\boldsymbol{r}$, of photon A. A judicious choice for θ can hence change the state into a superposition of symmetric and anti-symmetric Bell states (note that choosing $\theta = 0$ removes the phase and sets R to the identity rotation, i.e. the subspace

selector has no effect). In the absence of the BS in Fig. 1 b), it can be shown that the 'no beamsplitter', *nbs* state becomes

$$|\Psi_{nbs}\rangle = \sum_{\boldsymbol{r}\in\mathcal{S}} \frac{1}{\sqrt{d}} |\boldsymbol{r}\rangle_A |R(-2\theta)\boldsymbol{r}\rangle_B . \tag{2}$$

In this case, the outcome will match that of a conventional ghost imaging experiment, except with the measured image being rotated with respect to the original object (due to the rotated B photon state). This state is also symmetric. However, in the presence of the BS and properly matched paths lengths for A and B (i.e. a HOM filter) and post-selecting on coincidences between the two paths, it can be shown that the 'beamsplitter' state *bs* (see Ref. 13 for the derivation) is

$$|\Psi_{bs}\rangle = \mathcal{K} \sum_{\boldsymbol{r}\in\mathcal{S}} |\boldsymbol{r}\rangle_A \left[|R(-2\theta)\boldsymbol{r}\rangle_B - |R(2\theta)\boldsymbol{r}\rangle_B\right] . \tag{3}$$

with $\mathcal{K}$ an appropriate constant. This state can be shown to be anti-symmetric, and it is therefore predicted that ghost imaging with an HOM filter setup produces an image consisting of a juxtaposition of the original object rotated both by an angle 2θ and -2θ (a result of the two B photon states).

After preparing either $|\Psi_{nbs}\rangle$ or $|\Psi_{bs}\rangle$, the object/measurement part of the experiment is carried out using Spatial Light Modulators (SLMs) in both arms A and B instead of a spatially-resolved detector and a physical object. Firstly, the SLM in arm A of Fig. 1 b), $\mathrm{SLM_A}$, is masked with a binary object O of our choice and replaces the 'ghost' object. The information about said binary object is contained in a function $O(\boldsymbol{r})$: $O(\boldsymbol{r}) = 0$ if the pixel at position $\boldsymbol{r}$ in $\mathrm{SLM_A}$ is black in the object, and 1 if pixel $\boldsymbol{r}$ is white. In reality, the setup is aligned such that any light from the first order of the SLMs is coupled to avalanche photodiodes (APDs) after the object/measurement section. Hence 'black' here means light is not sent to the first order (and hence isn't detected), while 'white' means that light is sent to the first order. The operator used to describe this $\mathrm{SLM_A}$ masking process is $|O\rangle_A = \mathcal{N}\sum_{\boldsymbol{r}\in\mathcal{S}} O(\boldsymbol{r})|\boldsymbol{r}\rangle_A$, with $\mathcal{N}$ the appropriate normalization. After being masked with an object, $\mathrm{SLM_A}$ remains static for the duration of the experimental run.

Secondly, $\mathrm{SLM_B}$ is used to glean spatial information in arm B by performing a single-pixel scan: a single pixel at a specific transverse position $|\boldsymbol{r}\rangle_B$ is 'turned on' in $\mathrm{SLM_B}$ such that light incident on that pixel is coupled to the detector. Coincidences are then counted between the APDs in each arm for a pre-defined integration time. This process is repeated for every pixel $\boldsymbol{r}$. This coincidence count information allows the image to be reconstructed by taking a convex sum of all pixels with the weighting (intensity) of each pixel being proportional to the coincidence counts recorded for that pixel. As such, the intensity I of pixel $\boldsymbol{r}$ in the reconstructed object, in the case of the $|\Psi_{nbs}\rangle$ and $|\Psi_{bs}\rangle$ states in Eqs. (2) and (3), respectively, is

$$I_{nbs}(\boldsymbol{r}) \propto |O(R\boldsymbol{r})|^2 , \tag{4}$$

$$I_{bs}(\boldsymbol{r}) \propto \left|O(R\boldsymbol{r}) - O(R^{-1}\boldsymbol{r})\right|^2 , \tag{5}$$

where, as mentioned, R is the 2-dimensional rotation operation acting on the transverse position $\boldsymbol{r}$. These formula match the claim that the 'no beamsplitter' case corresponds to an image rotated with respect to the object, while the HOM filter 'beamplitter' case image is a combination of a rotated and counter-rotated object. In either case, the amount of rotation depends on θ, the relative angle between the Dove prisms in the subspace selector.

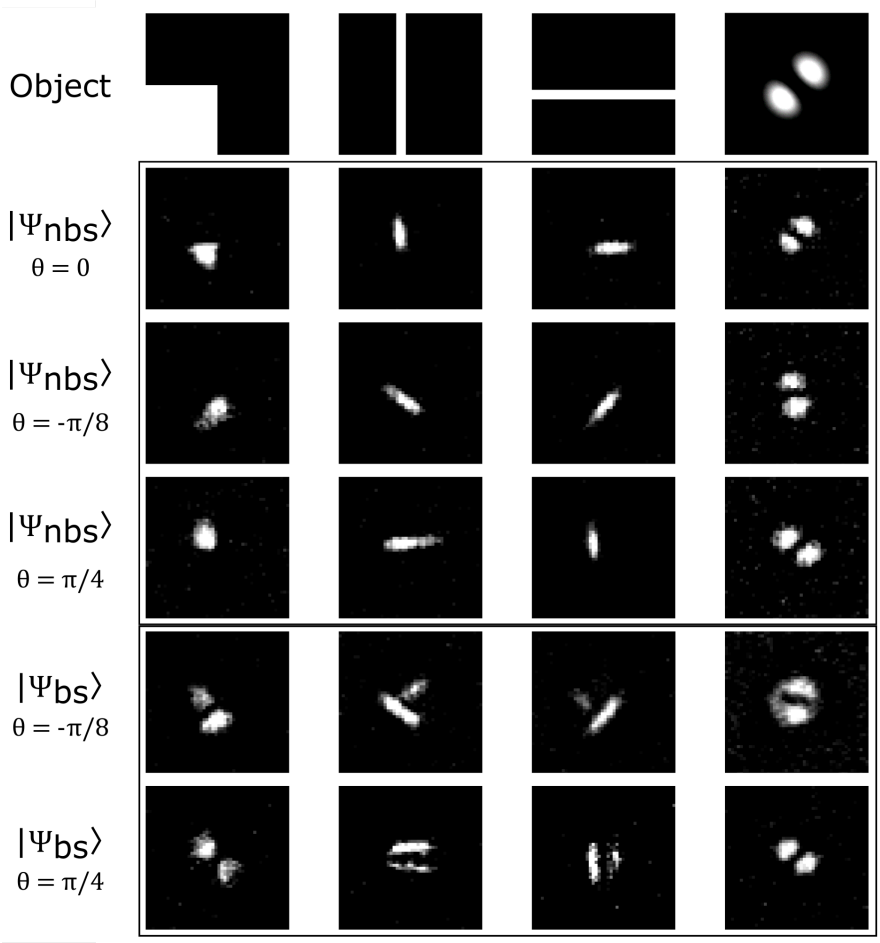

Figure 2. 2-way ghost imaging results. The original object is given in the first row and the corresponding results obtained under various state projections and filters are given in subsequent rows. Each column corresponds to the results obtained given the object atop the column.

2.2 Results and discussion

The experimental results, which accord with the theory presented here, are given in Fig. 2: post-selecting on symmetric states produces the original object (save for a possible rotation), whereas post-selecting on the anti-symmetric state produces the juxtaposed 'double' image. Note that, given a relative angle of θ between the two Dove prisms, the reconstructed image is rotated by an angle of 2θ with respect to the original object. Also, note interestingly that the $|\Psi_{bs}\rangle, \theta = \pi/4$ result in the last column of Fig. 2 is identical to the original object (again, up to a rotation). No 'image doubling' is observed, given the innate rotational symmetry of the object which isn't present in the other objects. Therefore, it is conceivable that such a test could be used in aligning highly sensitive setups, since any differences observed between the object and reconstructed image (in the case of an object with innate rotational symmetry) will be the result of imperfect alignment.

The juxtaposed image observed in the presence of an HOM filter could be chalked up to the anti-symmetric state, but could potentially also be understood as the beamsplitter 'splitting' the image in two, with the image parts being recombined after they are altered in their different respective paths. If photon B, which does not see the Dove prisms, is reflected by the beamsplitter and hence interacts with the object, the rotated photon A is measured by the single-pixel scan. However, if the rotated photon A is transmitted at the beamsplitter and interacts with the object, the un-rotated photon B is measured by the single-pixel scan. To distinguish between these two possible explanations, future studies might consider greatly increasing the path length of one arm (or equivalently, using a long fibre in one arm of the coincidence counter), which should distinguish the two cases.

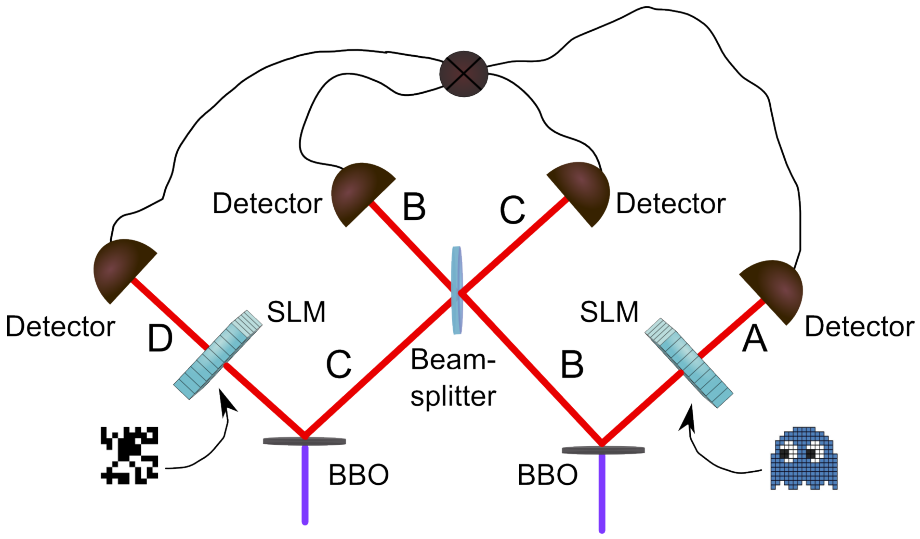

Figure 3. Schematic description of a 4-way ghost imaging setup.

However, Ref. 13 highlights the importance of further studying the role of quantum state symmetry in ghost imaging, as well as considering the intersection between imaging and spatially-engineered states of light.

3. 4-WAY IMAGING

3.1 Setup

State symmetry and projection has a further interesting effect on the reconstructed image in a 4-way ghost imaging setup, the schematic of which is given in Fig. 3 (the full study can be found in Ref. 12). This setup consists of two pairs of entangled photons, which are initially independent. By combining a photon from each pair and performing projective measurements on them, the remaining photons from each pair become entangled (entanglement swapping) and can subsequently be used to perform traditional ghost imaging.

Firstly, two SPDC sources create two pairs of completely independent entangled photons: pairs A/B and C/D. Again, in the position basis and assuming a flat-top beam, the initial state of the system is

$$|\Psi\rangle = \sum_{\boldsymbol{r}\in\mathcal{S}} \frac{1}{\sqrt{d}} |\boldsymbol{r}\rangle_A |\boldsymbol{r}\rangle_B \otimes \sum_{\boldsymbol{s}\in\mathcal{S}} \frac{1}{\sqrt{d}} |\boldsymbol{s}\rangle_C |\boldsymbol{s}\rangle_D \,, \tag{6}$$

where the two sums independently run over the d discrete transverse pixel positions $\boldsymbol{r}, \boldsymbol{s}$ the SLMs (which will again be used to construct the object and perform measurements) are comprised of. This is the case since the transverse positions of the photons in their respective crystals are relayed onto the SLM planes using lenses.

Next, photons B and C are combined in a BS, the action of which is[17]

$$|\boldsymbol{r}\rangle_B \to \frac{1}{\sqrt{2}} \left(|\boldsymbol{r}\rangle_B - |\boldsymbol{r}\rangle_C\right) \;;\; |\boldsymbol{r}\rangle_C \to \frac{1}{\sqrt{2}} \left(|\boldsymbol{r}\rangle_B + |\boldsymbol{r}\rangle_C\right). \tag{7}$$

Assuming a properly set up HOM filter (perfectly matched path lengths for arms B and C, and a BS combining the photons), the full state prior to any coincidence post-selection is

$$|\Psi\rangle = \frac{1}{2d} \sum_{\boldsymbol{r},\boldsymbol{s}\in\mathcal{S}} |\boldsymbol{r}\rangle_A |\boldsymbol{s}\rangle_D \left[|\boldsymbol{r},\boldsymbol{s}\rangle_B - |\boldsymbol{r},\boldsymbol{s}\rangle_C + |\boldsymbol{r}\rangle_B |\boldsymbol{s}\rangle_C - |\boldsymbol{s}\rangle_B |\boldsymbol{r}\rangle_C\right]. \tag{8}$$

Given this state, post-selecting on the presence (absence) of coincidences between detectors B and C has the net effect of filtering out the symmetric (anti-symmetric) part of Eq. (6), leaving behind only the anti-symmetric

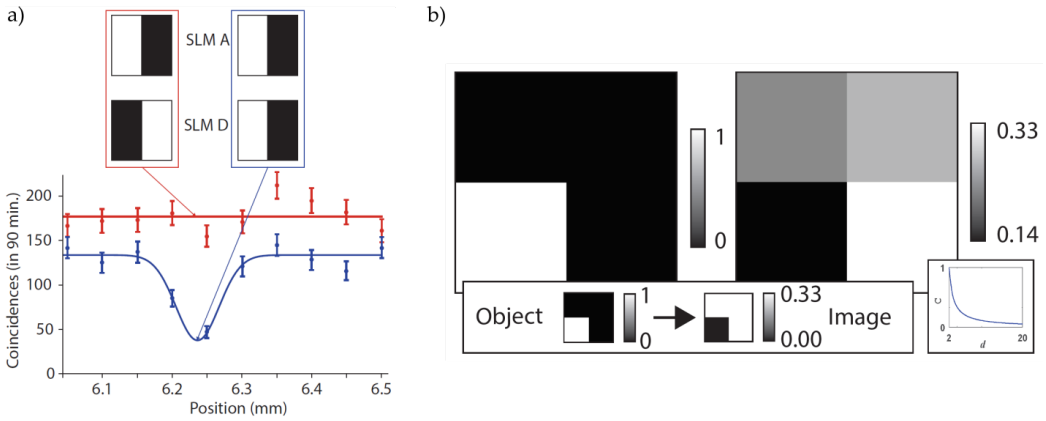

Figure 4. a) Plot of 4-way coincidences recorded as a function of the translation stage position. The counts recorded are higher in the contrast-reversed case. b) Experimental results (right) for a 4-pixel binary object (left). The bottom inset shows the theoretically-simulated results, with the small, bottom-left inset showing the contrast dependence (difference between white and black pixels) as a function of the image size (in pixels).

part, i.e. the third and fourth terms in square brackets in Eq. (6) (symmetric part (first and second terms)). After having made the choice of a post-selection scheme, the remaining photons in arms A and D can be employed in a ghost imaging setup analogous to that outlined in Section 2: $\mathrm{SLM_A}$ is masked with a binary object O (the information of which is contained in the same function $O(\boldsymbol{r})$ as before) and a single-pixel scan is carried out on $\mathrm{SLM_D}$, recording the transverse pixel position $|\boldsymbol{r}\rangle_D$ and the corresponding coincidence count. For example, if wishing to post-select on anti-symmetric states, one would post-select on coincidences in all four detectors. And, as before, the final image is reconstructed by taking a convex combination of all pixels weighted by the corresponding coincidence count.

As per Ref. 12, it is predicted that the intensity I of the pixel at transverse position $\boldsymbol{r}$ in the reconstructed image, in the case of projecting onto anti-symmetric (AS) and symmetric (S) subspaces, is

$$I_{AS}(\boldsymbol{r}) = \frac{B - O(\boldsymbol{r})}{2d^2} \; ; \; I_S(\boldsymbol{r}) = \frac{B + O(\boldsymbol{r})}{2d^2}, \tag{9}$$

where B is the total number of white 'on' pixels in the object O. Interestingly, note that, in the anti-symmetric case, the reconstructed image will be a 'contrast-reversed' version of the original object: if pixel $\boldsymbol{r}$ is white in the original binary object O, the corresponding pixel intensity in the image, $\frac{B-1}{2d^2}$, is less than if pixel $\boldsymbol{r}$ were black, $\frac{B}{2d^2}$. However, in the symmetric case, an image with the original contrast is expected: if pixel $\boldsymbol{r}$ is white in the object, the corresponding pixel intensity in the image, $\frac{B+1}{2d^2}$, is larger than if the pixel were black, $\frac{B}{2d^2}$.

3.2 Results and discussion

Fig. 4 a) gives two overlapped plots, with the corresponding SLM masks shown in the insets, each depicting the total number of 4-way coincidences (hence anti-symmetric post-selection) recorded in a 90 minute integration period versus the absolute position of a translation stage (which is used to match the lengths of paths B and C so as to create an HOM filter). Notice that when the path lengths are matched (i.e. at the stage position of roughly 6.24mm, the position coinciding with the 'dip' in the blue plot), many more coincidences are recorded when the mask on $\mathrm{SLM_D}$ is the contrast-reversed version of that on $\mathrm{SLM_A}$, compared with the case with the same contrast on both SLMs. Therefore, the reconstructed image is contrast-reversed with respect to the object, as anticipated. Indeed, Fig. 4 b) shows that the same contrast-reversal holds for higher-dimensional objects, although to a lesser degree: the difference between white and black pixels, i.e. the contrast (see Eq. 9), decreases as the object dimension increases. Therefore, the contrast between white and black pixels is most apparent for simple, 2-pixel objects.

The normalised reconstructed image in Fig. 4 b) can be compared with the theoretically-predicted image using the mean squared error (MSE)

$$\mathrm{MSE} = \frac{1}{d^2} \sum_{\boldsymbol{r} \in \mathcal{S}} \left[I(\boldsymbol{r}) - M(\boldsymbol{r}) \right]^2 , \tag{10}$$

where $I(\boldsymbol{r})$ is the measured intensity of pixel $\boldsymbol{r}$, and $M(\boldsymbol{r})$ is the predicted intensity. In this case, the MSE ranges from 0 (for a measured image perfectly matching the predicted image) to 1 for a completely dissimilar reconstructed image. For Fig. 4 b), we obtain MSE = 0.0078, which accords well with the theory set out above.

To conclude, Ref. 12 constitutes the first implementation of ghost imaging using independent photons and the first observed contrast reversal in ghost imaging. It would be interesting to consider an analogous, classical implementation of this experiment, since it is known that classical correlations are sufficient to observe ghost imaging.[4,18] However, no classical analog for projecting onto (anti-)symmetric states exists, and indeed, the quantum teleportation of spatial states of light cannot be replicated classically. Despite this, said findings suggest new aspects for traditional classical ghost imaging to consider; classical signaling processing protocols could also perhaps be employed with this work in mind to enhance the reconstructed images.

ACKNOWLEDGMENTS

N. B. acknowledges support from the South African CSIR DST-IBS programme, A. V. from the Claude Leon Foundation, A. F. from the NRF, and J. L. was supported by the Engineering and Physical Sciences Research Council through the Quantum Hub in Quantum Enhanced Imaging.

REFERENCES

[1] Pittman, T., Shih, Y., Strekalov, D., and Sergienko, A., "Optical imaging by means of two-photon quantum entanglement," *Physical Review A* **52**(5), R3429 (1995).

[2] Walborn, S. P., Monken, C., Pádua, S., and Ribeiro, P. S., "Spatial correlations in parametric down-conversion," *Physics Reports* **495**(4-5), 87–139 (2010).

[3] Bennink, R. S., Bentley, S. J., and Boyd, R. W., ""two-photon" coincidence imaging with a classical source," *Physical Review Letters* **89**(11), 113601 (2002).

[4] Bennink, R. S., Bentley, S. J., Boyd, R. W., and Howell, J. C., "Quantum and classical coincidence imaging," *Physical Review Letters* **92**(3), 033601 (2004).

[5] Erkmen, B. I. and Shapiro, J. H., "Ghost imaging: from quantum to classical to computational," *Advances in Optics and Photonics* **2**(4), 405–450 (2010).

[6] Katz, O., Bromberg, Y., and Silberberg, Y., "Compressive ghost imaging," *Applied Physics Letters* **95**(13), 131110 (2009).

[7] Ryczkowski, P., Barbier, M., Friberg, A. T., Dudley, J. M., and Genty, G., "Ghost imaging in the time domain," *Nature Photonics* **10**(3), 167 (2016).

[8] Jack, B., Leach, J., Romero, J., Franke-Arnold, S., Ritsch-Marte, M., Barnett, S., and Padgett, M., "Holographic ghost imaging and the violation of a bell inequality," *Physical Review Letters* **103**(8), 083602 (2009).

[9] Chan, K. W. C., O'Sullivan, M. N., and Boyd, R. W., "Two-color ghost imaging," *Physical Review A* **79**(3), 033808 (2009).

[10] Shapiro, J. H. and Boyd, R. W., "The physics of ghost imaging," *Quantum Information Processing* **11**(4), 949–993 (2012).

[11] Moreau, P.-A., Toninelli, E., Gregory, T., and Padgett, M. J., "Imaging with quantum states of light," *Nature Reviews Physics* **1**(1), 367–380 (2019).

[12] Bornman, N., Agnew, M., Zhu, F., Vallés, A., Forbes, A., and Leach, J., "Ghost imaging using entanglement swapped photons," *npj Quantum Information* **5** (7 2019).

[13] Bornman, N., Prabhakar, S., Vallés, A., Leach, J., and Forbes, A., "Ghost imaging with engineered quantum states by hong-ou-mandel interference," *New Journal of Physics* **21**, 073044 (jul 2019).

[14] Hong, C.-K., Ou, Z.-Y., and Mandel, L., "Measurement of subpicosecond time intervals between two photons by interference," *Physical Review Letters* **59**(18), 2044 (1987).

[15] Ndagano, B. and Forbes, A., "Entanglement distillation by hong-ou-mandel interference with orbital angular momentum states," *APL Photonics* **4**(1), 016103 (2019).
[16] Zhang, Y., Roux, F. S., Konrad, T., Agnew, M., Leach, J., and Forbes, A., "Engineering two-photon high-dimensional states through quantum interference," *Science advances* **2**(2), e1501165 (2016).
[17] Gerry, C., Knight, P., and Knight, P., [*Introductory Quantum Optics*], Cambridge University Press (2005).
[18] Valencia, A., Scarcelli, G., D'Angelo, M., and Shih, Y., "Two-photon imaging with thermal light," *Physical Review Letters* **94**(6), 063601 (2005).